

# Robust Preparation of Many-body Ground States in Jaynes-Cummings Lattices

Kang Cai,<sup>1</sup> Prabin Parajuli,<sup>1</sup> Guilu Long,<sup>2,3,4,5</sup> Chee Wei Wong,<sup>6</sup> and Lin Tian<sup>1,\*</sup>

<sup>1</sup>*School of Natural Sciences, University of California, Merced, California 95343, USA*

<sup>2</sup>*Beijing Academy of Quantum Information Sciences, Beijing 100193, China*

<sup>3</sup>*State Key Laboratory of Low-Dimensional Quantum Physics and Department of Physics, Tsinghua University, Beijing 100084, China*

<sup>4</sup>*Beijing National Research Center for Information Science and Technology  
and School of Information Tsinghua University, Beijing 100084, China*

<sup>5</sup>*Frontier Science Center for Quantum Information, Beijing 100084, China*

<sup>6</sup>*Electrical & Computer Engineering, and Center for Quantum Science & Engineering,  
University of California, Los Angeles, California 90095, USA*

Strongly-correlated polaritons in Jaynes-Cummings (JC) lattices can exhibit quantum phase transitions between the Mott-insulating and the superfluid phases at integer fillings. Here we present an approach for the robust preparation of many-body ground states of polaritons in a finite-sized JC lattice by optimized nonlinear ramping. In the deep Mott-insulating and deep superfluid regimes, polaritons can be pumped into a JC lattice and be prepared in the ground state with high accuracy via engineered pulse sequences. Using such states as initial state and employing optimized nonlinear ramping, we demonstrate that many-body ground states in the intermediate regimes of the parameter space can be generated with high fidelity. We exploit a Landau-Zener-type of estimation on this finite-sized system and derive an optimal ramping index for selected ramping trajectories, which greatly improves the fidelity of the prepared states. With numerical simulation of the ramping process, we further show that by choosing an appropriate trajectory, the fidelity can remain close to unity in almost the entire parameter space. This method is general and can be applied to many other systems.

## I. INTRODUCTION

The Jaynes-Cummings (JC) model is a prototype for studying light-matter interaction, where a quantum two-level system is coupled to a cavity mode [1]. This model has been utilized to study cavity or circuit quantum electrodynamics (QED) in a wide range of systems, from individual particles in the atomic scale to collective modes in mesoscopic devices [2–4]. More recently, advances in device fabrication and quantum technology enabled the exploration of novel many-body physics in arrays of JC models (i.e., JC lattices), which can be realized with optical cavities coupled to defects in semiconductors [5–9] and superconducting circuit QED systems [10–15]. The light-matter coupling in the JC models in the lattice induces intrinsic nonlinearity in the energy spectrum, which can be mapped to an onsite repulsive interaction between polariton excitations. The competition between this onsite interaction and the polariton hopping between neighboring sites gives rise to rich many-body physics for strongly-correlated polaritons in JC lattices, such as quantum or dissipative phase transitions and novel transport phenomena [16–18]. One effect of particular interest is the quantum phase transition between the Mott-insulating (MI) and the superfluid (SF) phases for polaritons at integer fillings of JC lattices, featured by the occurrence of off-diagonal long-range orders in correlation functions. It was shown that this effect can be observed in coupled cavity arrays [5–7] and multi-connected JC lattices [13–15].

The prerequisite to observe the MI-SF phase transition is to pump polariton excitations into a JC lattice and prepare them into appropriate ground states. However, preparing many-body ground states is a challenging task in engineered systems

such as quantum simulators [19–21] and adiabatic quantum computers [22, 23]. A number of approaches have been studied to tackle this problem, including adiabatic quantum evolution [24–26], quantum shortcut method with counter-diabatic interactions [27, 28], quantum phase estimation (QPE) via quantum Fourier transformation [29, 30], variational quantum eigensolver [31, 32], full quantum eigensolver [33], and engineered dissipative environment approach [34, 35]. Despite these efforts, it is still hard to generate desired many-body states with high fidelity in the noisy intermediate-scale quantum (NISQ) era [36], in particular, for systems working with excitations such as the JC lattices. The barriers to generating desired many-body states efficiently and accurately include the lack of a priori knowledge of the energy spectrum, the difficulty in engineering complicated counter-diabatic interactions, the rapid decrease of energy gaps and quick increase of the size of parametrized quantum circuits with the size of quantum simulators, and the limited decoherence times in NISQ devices. Furthermore, many-body states in strongly-correlated systems can be highly entangled, unknown, and hence, often impossible to be generated with pre-programmed quantum logic gates.

Here we study the robust generation of many-body ground states in a finite-sized JC lattice at unit filling using optimized nonlinear ramping. By adjusting its parameters to have no hopping between adjacent unit cells, or in the opposite limit, diminishing light-matter coupling, the JC lattice can be tuned to the deep MI or deep SF regimes, where the JC lattice is composed of uncoupled subsystems of individual unit cells or collective cavity modes. We show that polaritons can be pumped into the ground states of these limiting cases with high accuracy via engineered pulse sequences by using the approach developed in [37]. The number of pulses is  $O(N)$ , linear to the number of polaritons. With such states as initial state, we employ optimized nonlinear ramping to generate the

\* ltian@ucmerced.edu

many-body ground states in the intermediate regimes of the parameter space. In previous works [38–40], it was shown that nonlinear ramping can reduce diabatic transitions to excited states or the production of domain walls when a thermodynamic system evolves across the quantum critical point of a quantum phase transition due to the scaling of the many-body system. In this work, we apply nonlinear adiabatic ramping to a finite-sized system, where the energy gap between the ground and the excited states remains finite. By exploiting a Landau-Zener-type of estimation [41, 42] and the spectral feature along a given trajectory, we derive an optimal ramping index for the trajectory, which can significantly improve the fidelity of the prepared state. Our result agrees well with the data from numerical simulation of the ramping process. Furthermore, we show that by selecting an appropriate trajectory for a given set of target parameters combined with the optimal ramping index, the fidelity can remain close to unity in almost the entire parameter space.

Finite-sized JC lattices have been implemented in recent experiments [18, 43, 44] and the adiabatic evolution studied here is within reach of current technology [45–47]. Using practical parameters from recent experiments, we estimate that high fidelity can be achieved for the final states on a time scale much shorter than the observed decoherence times of these devices. The method of optimized nonlinear ramping for finite-sized systems is general and can be applied to many other problems. This work can hence guide future works on high-fidelity preparation of many-body states and observation of many-body correlations in quantum simulators.

This paper is organized as follows. In Sec. II, we introduce the Hamiltonian of a one-dimensional (1D) JC lattice and the MI-SF phase transition in this model. In Sec. III, we show that polaritons can be pumped into the JC lattice and prepared in the ground states of the deep MI and SF regimes. We then employ optimized nonlinear ramping to prepare the many-body ground states in the intermediate regimes of the parameter space in Sec. IV. We derive the optimal ramping index for given trajectories and compare this result with data from numerical simulation. In Sec. V, we discuss the improvement of the final-state fidelity by choosing an appropriate ramping trajectory and the total evolution time for practical devices. Conclusions are given in Sec. VI.

## II. QUANTUM PHASE TRANSITION IN JC LATTICE

Consider the JC lattice depicted in Fig. 1(a). Here each unit cell contains a qubit coupled to a cavity mode with coupling strength  $g$ , and adjacent unit cells are connected via photon hopping with hopping rate  $J$ . The total Hamiltonian of this model is  $H_t = H_0 + H_{int}$  ( $\hbar = 1$ ), where

$$H_0 = \omega_c \sum_j a_j^\dagger a_j + \omega_z \sum_j \frac{\sigma_{jz} + 1}{2} + g \sum_j (a_j^\dagger \sigma_{j-} + \sigma_{j+} a_j) \quad (1)$$

is the Hamiltonian of uncoupled JC models with  $\omega_c$  the frequency of cavity modes,  $\omega_z$  the level splitting of the qubits,  $a_j$  ( $a_j^\dagger$ ) the annihilation (creation) operator of the  $j$ -th cavity, and

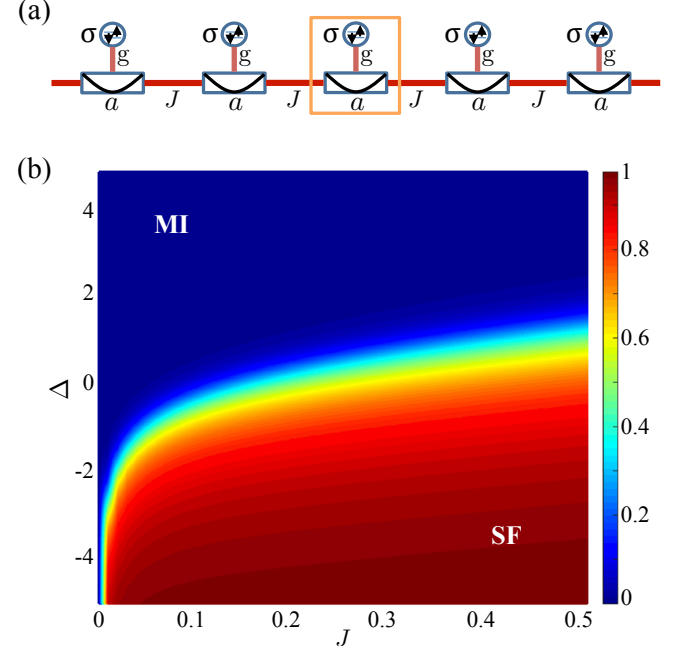


FIG. 1. (a) Schematic of a 1D JC lattice. Circles (rectangles) represent qubits (cavity modes) with light-matter coupling  $g$  and hopping rate  $J$ . (b) Single-particle density matrix  $\rho_1(1,4)$  vs hopping rate  $J$  and detuning  $\Delta$  for a finite-sized lattice with  $N = L = 6$ . Here we let  $g \equiv 1$  as the energy unit.

$\sigma_{j\pm}, \sigma_{jz}$  the Pauli operators of the  $j$ -th qubit, and

$$H_{int} = -J \sum_j (a_j^\dagger a_{j+1} + a_{j+1}^\dagger a_j) \quad (2)$$

is the photon hopping between neighboring unit cells. Let  $\{|n, s\rangle\}$  be the basis set of an individual JC model with the cavity in the Fock state  $n$  and the qubit in the state  $s = \uparrow, \downarrow$ . The eigenstates of the JC model include the ground state  $|g_0\rangle = |0, \downarrow\rangle$  with no excitation and the polariton doublets  $|n, \pm\rangle$  with integer number  $n$  excitations, where

$$|n, +\rangle = \cos(\theta/2) |n, \downarrow\rangle + \sin(\theta/2) |n-1, \uparrow\rangle, \quad (3)$$

$$|n, -\rangle = \sin(\theta/2) |n, \downarrow\rangle - \cos(\theta/2) |n-1, \uparrow\rangle \quad (4)$$

with  $\theta = 2 \arcsin \sqrt{[1 - \Delta/\chi(n)]/2}$ ,  $\chi(n) = \sqrt{\Delta^2 + 4ng^2}$ , and  $\Delta = \omega_c - \omega_z$  the detuning between the cavity mode and the qubit. The corresponding eigenenergies are  $E_{g_0} = 0$  and  $E_{n,\pm} = (n - 1/2)\Delta \pm \chi(n)/2$ . When the coupling  $g$  is nonzero, the energy spacings between the eigenstates become unequal with  $(E_{n+1,-} - E_{n,-}) > (E_{n,-} - E_{n-1,-})$ . Specifically,  $E_{2,-} > 2E_{1,-}$  for  $n = 1$ , which indicates that the energy to add two polaritons to the JC model is more than twice the energy to add a single polariton. The extra energy to add a second polariton can be viewed as an effective onsite interaction or nonlinearity of the polaritons, which is at the root of many interesting phenomena in JC models or lattices, such as the photon blockade effect [5–7] and electron-phonon-like effect [48].

In the limit of  $J = 0$ , the JC lattice is composed of isolated JC models. The ground state at unit filling, where the number

of polaritons  $N$  is equal to the number of lattice sites  $L$ , is

$$|G\rangle_{J=0} = \prod_j |1, -\rangle_j \quad (5)$$

with one polariton excitation occupying the state  $|1, -\rangle$  at each site, which is in the deep MI regime. States with more than one excitations at the same site are energetically unfavorable due to the onsite interaction. In the opposite limit of  $g = 0$  and finite hopping rate  $J$ , the cavity modes are decoupled from the qubits. The hopping Hamiltonian (2), now the dominant term, can be transformed to the momentum space under the periodic boundary condition with  $H_{int} = -2J \sum_k \cos(k) a_k^\dagger a_k$ , where  $a_k = \sum_j a_j e^{ik \cdot j} / \sqrt{N}$  ( $a_k^\dagger$ ) is the annihilation (creation) operator of a collective cavity mode at quasimomentum  $k = \pi m/N$  with integer number  $m \in [-(N-1), N]$ . At  $\Delta < 0$  with the cavity frequency below the qubit energy, the ground state at unit filling is

$$|G\rangle_{g=0} = \frac{1}{\sqrt{N!}} \left( a_{k=0}^\dagger \right)^N \prod_j |0, \downarrow\rangle_j \quad (6)$$

with all polaritons occupying the mode  $a_{k=0}$ , which is a non-local state in the deep SF regime.

With the mean-field approximation [5–7] and numerical methods [8, 9, 13–15], it was shown that quantum phase transitions between the MI and SF phases due to the competition between the onsite interaction and the photon hopping can occur in the intermediate regimes of the parameter space of a JC lattice. For a finite-sized lattice with  $N = L = 6$ , we numerically calculate the many-body ground states using the exact diagonalization method. The spatial correlation in the many-body ground state  $|G\rangle$  can be characterized by the normalized single-particle density matrix defined as [49, 50]

$$\rho_1(i, j) = \langle G | a_i^\dagger a_j | G \rangle / \langle G | a_i^\dagger a_i | G \rangle, \quad (7)$$

which reveals the off-diagonal long-range order of the state. The single-particle density matrix decreases algebraically with the spatial separation  $|i - j|$  in the SF phase and decreases exponentially in the MI phase [13–15]. For a finite  $|i - j|$ ,  $\rho_1(i, j)$  of the SF phase is much larger than that of the MI phase. In Fig. 1(b), we plot our numerical result of  $\rho_1(1, 4)$  as functions of the hopping rate  $J$  and the detuning  $\Delta$ , with  $g \equiv 1$  as the energy unit. It can be seen that  $\rho_1(1, 4)$  increases with  $J$  for an arbitrary detuning. In the deep MI regime with  $J = 0$ ,  $\rho_1(1, 4) = 0$  with the polaritons localized in the lattice. In the deep SF regime,  $\rho_1(1, 4)$  can approach unity. This result clearly indicates the occurrence of the MI-SF phase transition. Meanwhile, in this finite-sized system, the energy separation between the ground and the excited states decreases as the parameters approach the intermediate regimes, but maintains a finite energy gap.

### III. STATE INITIALIZATION

In this section, we present the methods to pump  $N = L$  polaritons to the JC lattice in the limiting cases of  $J = 0$  and

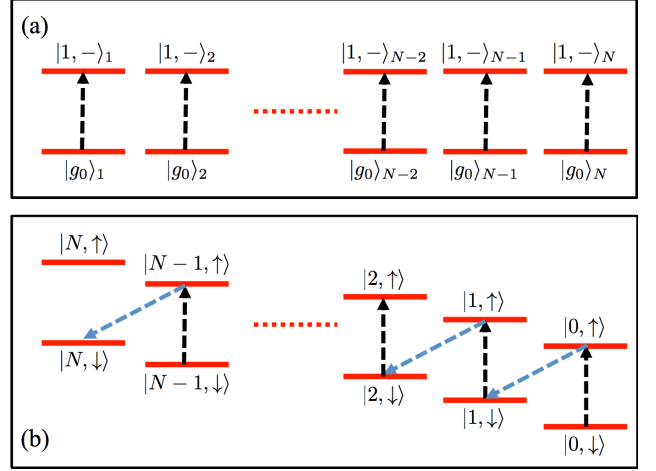


FIG. 2. Engineered pulses for state initialization at (a)  $J = 0$  and (b)  $g = 0$ . In (a), vertical arrows are Rabi flips between states  $|g_0\rangle$  and  $|1, -\rangle$  of JC models. In (b), vertical (slant) arrows are the operations  $C_l (Q_l)$  with  $l \in [1, N]$  on the auxiliary qubit and mode  $a_{k=0}$ .

$g = 0$ , respectively, by applying engineered pulses. The polaritons are pumped into the many-body ground states at the corresponding parameters. These states will be used as the initial state in the ramping process studied in Sec. IV.

#### A. Deep MI regime

At  $J = 0$ , the ground state is given by (5) with each unit cell in the polariton state  $|1, -\rangle$ . Because the unit cells are decoupled, we can perform a Rabi rotation between the states  $|g_0\rangle$  and  $|1, -\rangle$  on individual JC models, as illustrated in Fig. 2(a). The driving Hamiltonian can have the form  $H_{d1}(t) = \sum_j [\epsilon \exp^{i\omega_L t} \sigma_j^- + h.c.]$  with  $\epsilon$  the driving amplitude and  $\omega_L = E_{1,-} - E_{g_0}$  the driving frequency. The corresponding Rabi frequency can be derived as  $\Omega_{d1} = |\epsilon \cos(\theta/2)|$  following Eq. (4). The duration of the Rabi flip from the initial state  $|g_0\rangle$  to the final state  $|1, -\rangle$  is  $\tau_{d1} = \pi/2\Omega_{d1}$ . To prevent the driving pulse from inducing unwanted transitions to higher states such as  $|1, +\rangle$ , it requires that  $|\epsilon| \ll g$ .

#### B. Deep SF regime

In the opposite limit of  $g = 0$  and finite  $J$ , the ground state is given by (6) with all polaritons occupying the collective (nonlocal) mode  $a_{k=0}$ . To generate this state, we introduce an auxiliary qubit with Pauli operators  $\sigma_{0\pm}$ ,  $\sigma_{0z}$  and Hamiltonian

$$H_{d2}(t) = \frac{\omega_0}{2} \sigma_{0z} + \epsilon(t) e^{i\omega_L t} \sigma_{0-} + g_d(t) \sum_j a_j^\dagger \sigma_{0-} + h.c., \quad (8)$$

which includes the qubit energy term with frequency  $\omega_0$ , a driving on the qubit with amplitude  $\epsilon(t)$  and frequency  $\omega_L$ , and a time-dependent coupling between the qubit and mode  $a_{k=0}$  with coupling strength  $g_d(t)$ . With  $\omega_L, \omega_0 = \omega_c - 2J$

in resonance with mode  $a_{k=0}$ , we have  $H_{d_2}(t) = \epsilon(t)\sigma_{0-} + \sqrt{N}g_d(t)a_{k=0}^\dagger\sigma_{0-} + h.c.$  in the rotating frame. The first term of  $H_{d_2}$  generates a Rabi rotation on the auxiliary qubit, and the second term is a coupling between the qubit and mode  $a_{k=0}$ . Both terms can be tuned on and off within nanoseconds, as has been demonstrated in recent experiments on superconducting transmon qubits [43, 44].

With the qubits in the JC lattice decoupled from the cavities, the initial state of the coupled system of mode  $a_{k=0}$  and the auxiliary qubit is  $|0, \downarrow\rangle$ . To generate the state (6), we utilize the approach in [37] to design a pulse sequence by switching  $\epsilon(t)$  and  $g_d(t)$  on and off alternately. The unitary operator for this pulse sequence is

$$U = Q_N C_N Q_{N-1} C_{N-1} \cdots Q_2 C_2 Q_1 C_1, \quad (9)$$

where the unitary operator  $C_l$  ( $l \in [1, N]$ ) incurs a Rabi flip on the auxiliary qubit by applying a driving pulse with finite amplitude  $\epsilon$  ( $g_d = 0$ ) for a duration of  $\tau_{cl} = \pi/2|\epsilon|$ , and the unitary operator  $Q_l$  causes the exchange of excitations between the auxiliary qubit and mode  $a_{k=0}$  by turning on the coupling  $g_d$  ( $\epsilon = 0$ ) for a duration of  $\tau_{ql} = \pi/2\sqrt{Nl}|g_d|$ . Following this pulse sequence, the state evolves as  $|0, \downarrow\rangle \rightarrow |0, \uparrow\rangle \rightarrow |1, \downarrow\rangle \cdots \rightarrow |N, \downarrow\rangle$ , as shown in Fig. 2(b). The total duration of this pulse sequence is  $\tau_{d2} = \sum_l (\tau_{cl} + \tau_{ql})$ . Assuming that the magnitudes of  $\epsilon$  and  $g_d$  are fixed, we find  $\tau_{d2} = N\pi/2|\epsilon| + \sum_l \pi/2\sqrt{Nl}|g_d|$ , which increases with the number of polaritons as  $\tau_{d2} = O(N)$ . Meanwhile, it requires that  $|\epsilon|, \sqrt{N}|g_d| \ll \omega_L$  to achieve high fidelity for the final state. Note that at  $g = 0$  the JC lattice has other collective modes  $a_{k \neq 0}$ , which are separated from mode  $a_{k=0}$  only by a frequency difference of  $\pi^2 J/N^2$ . But couplings between the auxiliary qubit and modes  $a_{k \neq 0}$  during the pulse sequence are prohibited by the symmetry of the Hamiltonian  $H_{d_2}$ .

#### IV. OPTIMIZED NONLINEAR RAMPING

Many-body ground states in the intermediate regimes of the parameter space cannot be calculated analytically, and we cannot design quantum logic operations to generate such states, in contrast to the ground states in the deep MI or SF regimes. In this section, we employ optimized nonlinear ramping to reach such states via adiabatic evolution.

##### A. Ramping trajectory and optimal index

In this scheme, a parameter  $p$  has the time dependence:

$$p(t) = p(0)[1 - (t/T)^r] + p(T)(t/T)^r, \quad (10)$$

where  $p = g, J, \Delta$  is a tunable parameter of the JC lattice,  $p(0)$  is the initial value of the parameter at time  $t = 0$ ,  $p(T)$  is the target value at the final time  $T$ , and  $r$  is the ramping index. For  $r = 1$ , it is the linear ramping studied in adiabatic quantum computing [22, 23]; and  $r \neq 1$  corresponds to nonlinear

ramping [38–40]. It can be shown that for any two parameters at an arbitrary time  $t$ , e.g.,

$$\frac{\Delta(t) - \Delta(0)}{\Delta(T) - \Delta(0)} \equiv \frac{J(t) - J(0)}{J(T) - J(0)}. \quad (11)$$

Hence the evolution trajectory in the parameter space is independent of the ramping index  $r$  for given initial and target values of the parameters. On the other hand, the ramping index can strongly affect the sweeping rate of the Hamiltonian along a trajectory. Using (10), we obtain the time derivative  $p' = dp(t)/dt$  as a function of  $p$ :

$$p'(p) = \frac{r[p - p(0)]^{(r-1)/r}}{T[p(T) - p(0)]^{-1/r}}. \quad (12)$$

The sweeping rate of the Hamiltonian at a given set of parameters  $\{p\}$  can be written as  $\langle dH/dt \rangle = \sum_p \langle \partial H / \partial p \rangle p'(p)$ , which depends on  $r$  via  $p'(p)$ , with  $\langle \cdot \rangle$  the operator average at the ground state of parameters  $\{p\}$ .

Let  $|\psi(T)\rangle$  be the wave function of the final state of the evolution at time  $T$ . The fidelity of the final state can be defined as  $F = |\langle \psi(T) | G_T \rangle|^2$  with  $|G_T\rangle$  the many-body ground state at the target parameters  $\{p(T)\} = \{g(T), J(T), \Delta(T)\}$ . During a continuous evolution, the probability of diabatic transitions can be approximated by the Landau-Zener formula  $\sim e^{-\pi E_{\text{gp}}^2/2H'_{\text{gp}}}$  [41, 42], where the energy gap  $E_{\text{gp}}$  is defined as the minimum of the energy separation between the ground and the excited states along the evolution trajectory, and  $H'_{\text{gp}}$  denotes sweeping rate of the Hamiltonian at the parameters of the energy gap. To reach the desired state with high fidelity, the adiabatic criterion, a commonly expressed as  $H'_{\text{gp}} \ll E_{\text{gp}}^2$ , needs to be satisfied so that the diabatic transitions are negligible. For a given trajectory, we can optimize the ramping index  $r$  to minimize  $H'_{\text{gp}}$  so as to suppress the diabatic transitions in the most vulnerable region of the evolution and greatly improve the fidelity of the final state. With (11) and (12), we find that  $H'_{\text{gp}} \propto r \{ [p(T) - p(0)] / [p_{\text{gp}} - p(0)] \}^{1/r}$  with  $p_{\text{gp}}$  the value of parameter  $p$  at the energy gap. At the optimal ramping index  $r_{\text{min}}$ ,  $\partial H'_{\text{gp}} / \partial r = 0$ . This leads to

$$r_{\text{min}} = \log \left[ \frac{p(T) - p(0)}{p_{\text{gp}} - p(0)} \right], \quad (13)$$

which only depends on the initial and final values of the trajectory and the position of the energy gap.

Below we will conduct numerical simulation on two trajectories to calculate the fidelity of the final state and compare the above result with the numerical data.

##### B. Trajectory I: from deep MI regime

We first consider a trajectory following (10) with  $g(t) \equiv 1$ ,  $\Delta(t) \equiv 0$ ,  $J(0) = 0$ , and  $J(T) \in [0, 0.5]$ , where the photon hopping rate is continuously increased from zero to a finite value. The initial state is (5) in the deep MI phase. Using the exact diagonalization method, we calculate the eigenstates and

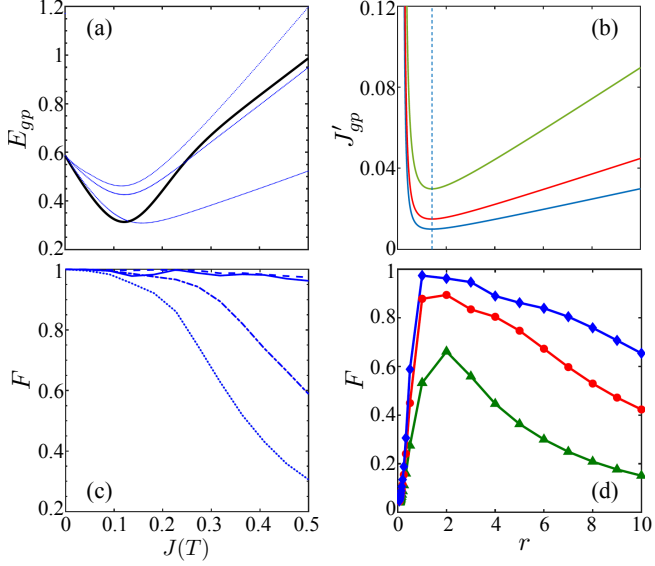


FIG. 3. (a) Energy spectrum of the lowest excited states vs hopping rate  $J(T)$ . Solid (dotted) curve is for the symmetric (asymmetric) state. Here  $g \equiv 1$ ,  $\Delta \equiv 0$ , and the ground-state energy is set to zero. (b) Time derivative  $J'_{gp}$  vs ramping index  $r$  at  $T = 5\pi/g, 10\pi/g, 15\pi/g$  from top to bottom, and  $J(T) = 0.5$ . (c) Fidelity  $F$  vs  $J(T)$  for  $r = 2$  (solid),  $1$  (dashed),  $1/2$  (dot-dashed), and  $1/3$  (dotted) at  $T = 15\pi/g$ . (d) Fidelity  $F$  vs  $r$  at  $T = 5\pi/g, 10\pi/g, 15\pi/g$  from bottom to top, and  $J(T) = 0.5$ .

eigenenergies of the JC lattice along this trajectory. The energy spectrum of the lowest excited states is plotted as a function of the hopping rate  $J(T)$  in Fig. 3(a). The solid curve corresponds to the energy of a state that is symmetric with regard to all lattice sites, and the dotted curves are for asymmetric states. As both the initial state and the Hamiltonian  $H(t)$  are symmetric with regard to lattice sites, the wave function  $|\psi(t)\rangle$  at an arbitrary time  $t$  must remain symmetric. Hence diabatic transitions can only happen between the ground state and this symmetric state, and the energy gap related to the adiabatic criterion is also determined by the energy separation between these two states. From our numerical result, we find that the energy gap occurs at  $J_{gp} = 0.122$  with  $E_{gp} = 0.31$ .

With this trajectory, the sweeping rate of the Hamiltonian  $H'_{gp} \propto J'_{gp}$  with  $J'_{gp}$  the time derivative of the hopping rate at the gap position. Using (12), we have

$$J'_{gp} = \frac{r J_{gp}^{(r-1)/r}}{T [J(T)]^{-1/r}}, \quad (14)$$

which is plotted as a function of  $r$  in Fig. 3(b). The derivative  $J'_{gp}$  contains a local minimum at the optimal ramping index  $r_{\min} = \log [J(T)/J_{gp}]$ . With the above parameters and  $J(T) = 0.5$ ,  $r_{\min} = 1.41$ , which indicates that the best fidelity for the final state can be achieved between linear and quadratic ramping. Using (14), we obtain  $J'_{gp} = 0.01$  at a total evolution time  $T = 15\pi/g$ . With the gap energy  $E_{gp} = 0.31$ , the adiabatic criterion is well satisfied. Meanwhile,  $J'_{gp}$ , and hence the probability of diabatic transitions, increase with the target value  $J(T)$ . We numerically simulate the ramping process

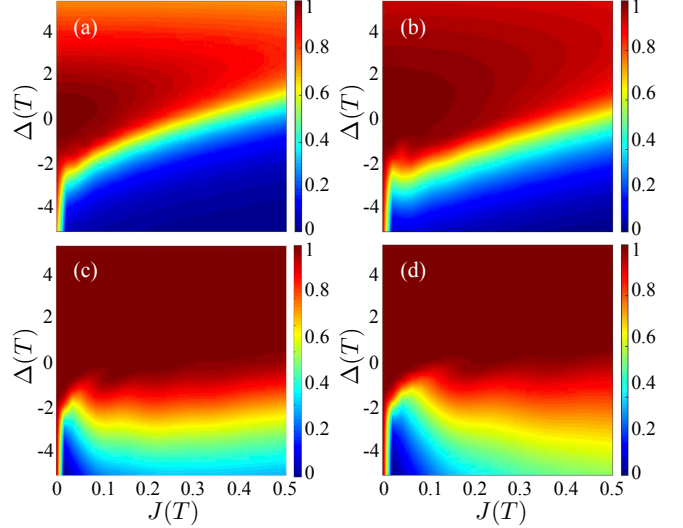


FIG. 4. Fidelity  $F$  vs target parameters  $J(T)$  and  $\Delta(T)$  for (a)  $r = 1/3$ , (b)  $r = 1/2$ , (c)  $r = 1$ , and (d)  $r = 2$ . Here  $g(t) \equiv 1$ ,  $J(0) = \Delta(0) = 0$  with trajectory (10), and  $T = 15\pi/g$ .

along this trajectory and calculate the fidelity of the final state. In Fig. 3(c), the fidelity vs  $J(T)$  is plotted for several values of ramping index  $r$  at  $T = 15\pi/g$ . The fidelity decreases quickly as  $J(T)$  becomes larger due to the increase of  $J'_{gp}$ . It can also be seen that for  $J(T)$  sufficiently larger than the value at the energy gap, the fidelity is much higher for  $r = 1, 2$  than that for  $r = 1/3, 1/2$ . As shown in Fig. 3(d), maximal fidelity is achieved when  $r \in (1, 2)$ , which agrees well with our result of the optimal ramping index.

Using numerical simulation, we obtain the fidelity of the final state for a wide range of target parameters following the trajectories of  $g(t) \equiv 1$ ,  $J(0) = \Delta(0) = 0$ , and finite values of  $J(T), \Delta(T)$  with the MI initial state (5). The fidelity is presented in Fig. 4(a-d) for  $r = 1/3, 1/2, 1, 2$ , respectively, at  $T = 15\pi/g$ . It can be seen that the fidelity decreases as the target parameters move further towards the SF phase. In particular, the fidelity exhibits a sharp drop when the parameters enter the SF phase crossing the energy gap. Meanwhile, the fidelity demonstrates strong dependence on the ramping index in the intermediate regimes of the parameter space, which agrees with our analytical prediction above.

### C. Trajectory II: from deep SF regime

Now we consider a trajectory that starts from the deep SF phase with  $g(0) = 0$ ,  $g(T) = 1$ ,  $J(0) = 0.5$ ,  $J(T) \in [0, 0.5]$ , and  $\Delta(t) \equiv 0$ , and follows the time dependence in (10) with initial state (6). In Fig. 5(a), we plot the energy spectrum of the lowest excited states vs the hopping rate  $J(T)$ . The solid curve is for a symmetric state and the dotted curves are for asymmetric states with regard to all lattice sites. As discussed in Sec. IV B, the ground state can only make diabatic transitions to the symmetric state, and the wave function of the quantum state will remain symmetric during the entire evo-

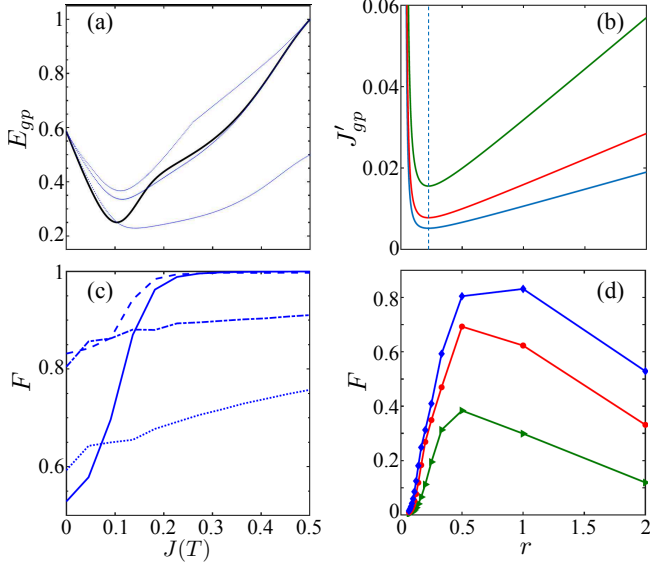


FIG. 5. (a) Energy spectrum of the lowest excited states vs hopping rate  $J(T)$ . Solid (dotted) curve is for the symmetric (asymmetric) state. Here  $g(0) = 0$ ,  $g(T) = 1$ ,  $J(0) = 0.5$ ,  $\Delta \equiv 0$ , and the ground-state energy is set to zero. (b) Time derivative  $J'_gp$  vs ramping index  $r$  at  $T = 5\pi/g, 10\pi/g, 15\pi/g$  from top to bottom, and  $J(T) = 0$ . (c) Fidelity  $F$  vs  $J(T)$  for  $r = 2$  (solid), 1 (dashed), 1/2 (dot-dashed), and 1/3 (dotted) at  $T = 15\pi/g$ . (d) Fidelity  $F$  vs  $r$  at  $T = 5\pi/g, 10\pi/g, 15\pi/g$  from bottom to top, and  $J(T) = 0$ .

lution. From our numerical result, the energy gap occurs at  $J_{gp} = 0.101$  with  $E_{gp} = 0.25$  along this trajectory.

The sweeping rate of the Hamiltonian  $H'_{gp} = g'_{gp}I_g - J'_{gp}I_J$  with  $g'_{gp}$  the time derivative of the coupling  $g$  at the gap position,  $I_g = \langle \sum_j (a_j^\dagger \sigma_{j-} + \sigma_{j+} a_j) \rangle$ , and  $I_J = \langle \sum_j (a_j^\dagger a_{j+1} + a_{j+1}^\dagger a_j) \rangle$ . Using (11), we have

$$g'_{gp} = \frac{g(T)}{T} rb^{1/r}, \quad (15)$$

$$J'_{gp} = \frac{J(T) - J(0)}{T} rb^{1/r} \quad (16)$$

with  $b = g(T)/g_{gp} = [J(T) - J(0)] / [J_{gp} - J(0)]$ . Hence  $H'_{gp}$  depends on the ramping index as  $rb^{1/r}$ , and the optimal ramping index can be derived as  $r_{\min} = \log(b)$ . With the above parameters and  $J(T) = 0$ , we have  $r_{\min} = 0.225$ , as shown in Fig. 5(b). Note that for different values of  $J(T)$ , the trajectory in the parameter space will be different, which results in different gap positions  $g_{gp}, J_{gp}$  and different  $r_{\min}$ . We numerically simulate the ramping process and obtain the fidelity of the final state vs the target hopping rate, as plotted in Fig. 5(c). The fidelity decreases as  $J(T)$  decreases away from  $J(0)$ , because  $|J'_{gp}|$  increases with the difference  $|J(T) - J(0)|$ . As  $J(T) \rightarrow 0$ , the fidelity for  $r = 1, 1/2$  is much higher than that for  $r = 2, 1/3$ . In Fig. 5(d), we plot the fidelity vs the ramping rate for  $J(T) = 0$ , which indicates that the best fidelity can be achieved for  $r \in (1/2, 1)$  at  $T = 10\pi/g, 15\pi/g$  and for  $r \in (1/3, 1/2)$  at  $T = 5\pi/g$ . This result confirms our estimation that the optimal ramping index of this trajectory

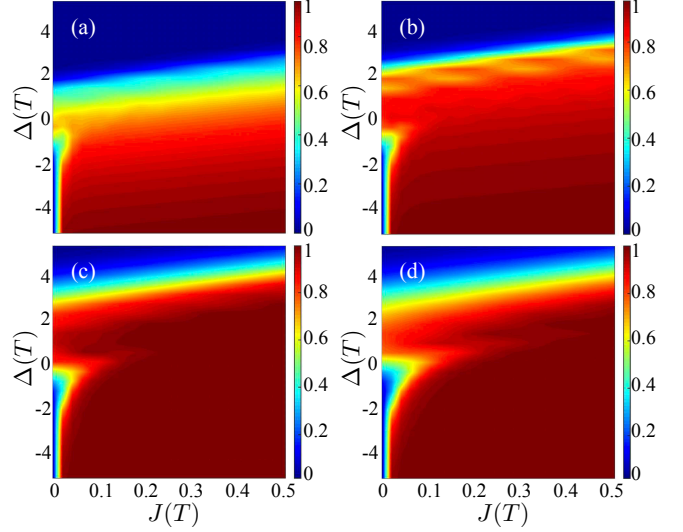


FIG. 6. Fidelity  $F$  vs target parameters  $J(T)$  and  $\Delta(T)$  for (a)  $r = 1/3$ , (b)  $r = 1/2$ , (c)  $r = 1$ , and (d)  $r = 2$ . Here  $g(0) = \Delta(0) = 0$ ,  $g(T) = 1, J(0) = 0.5$  with trajectory (10), and  $T = 15\pi/g$ .

will shift to a smaller value with  $r_{\min} \leq 1$  in comparison with that of Sec. IV B. The discrepancy between the numerical result and our estimation of  $r_{\min}$  could be owing to the small separation between the gap position and the target value, which will affect the accuracy of the Landau-Zener formula in adiabatic processes [41, 42].

We also obtain the fidelity of the final state for a wide range of target parameters following the trajectory (10) with  $g(0) = \Delta(0) = 0$ ,  $g(T) = 1$ ,  $J(0) = 0.5$ , finite values of  $J(T), \Delta(T)$ , and the SF initial state (6), as given in Fig. 6 for  $r = 1/3, 1/2, 1, 2$ , respectively, at  $T = 15\pi/g$ . The numerical result shows that the fidelity decreases quickly as the target parameters enter the MI phase and strongly depends on the ramping index in certain regimes of the parameter space.

## V. DISCUSSIONS

In Sec. IV, we showed that the fidelity of the final state in intermediate regimes of the parameter space can be greatly improved by choosing an optimal ramping index for a chosen trajectory and by increasing the total ramping time  $T$ . Here we show that for a given set of target parameters, the choice of the trajectory can have dramatic impact too. When the target parameters are in the MI phase, it is better to start from an initial state in the deep MI regime such as (5) so that the adiabatic evolution does not need to cross the energy gap to reach the target parameters and diabatic transitions remain negligible. Similarly, when the target parameters are in the SF phase, we can choose the initial state to be in the deep SF regime such as (6). For illustration, in Fig. 7, we plot the maximal fidelity from the two trajectories described in Sec. IV B [Fig. 4(c) for  $r = 1$ ] and in Sec. IV C [Fig. 6(c) for  $r = 1$ ], respectively. Compared with the plots in Fig. 4 and Fig. 6, the maximal fidelity remains close to unity in almost the entire parameter

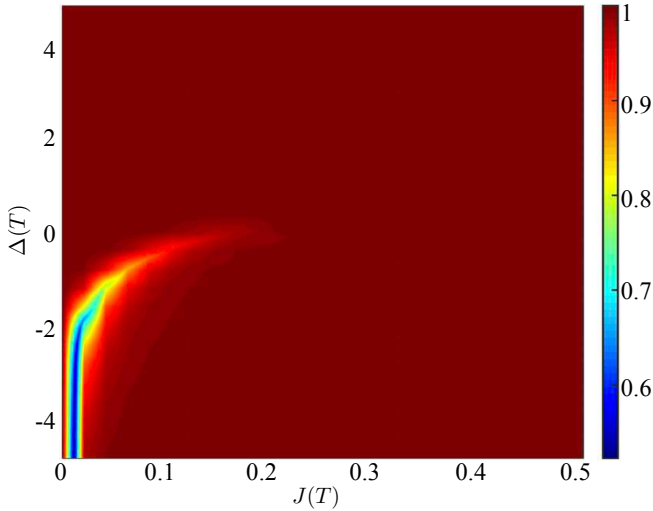


FIG. 7. Maximal fidelity vs target parameters  $J(T)$  and  $\Delta(T)$  from the two trajectories in Fig. 4(c) and Fig. 6(c), respectively.

space. Further improvement could be achieved by optimizing the trajectory to the target parameters.

An obvious approach to improve the fidelity of adiabatic processes is to increase the ramping time  $T$ , which can reduce the time derivative  $p'_{\text{gp}}$  and the sweeping rate of the Hamiltonian. This can be seen from the numerical result in Fig. 3(d) and Fig. 5(d). For quantum devices in the NISQ era, however, the decoherence times of the qubits and the cavity modes in a JC lattice set limits on the total evolution time. The many-body ground state studied here works with finite number of polariton excitations. In the presence of decoherence, the excitations can decay in a timescale comparable to the decoherence times. The ramping time needs to be much shorter than the decoherence times. In experiments, superconducting resonator cavities with frequency  $\omega_c/2\pi \sim 5$  GHz and quality factor  $10^5$  can be readily realized, which have a decay time of  $3\ \mu\text{sec}$ , and superconducting qubits can have a decoherence time of  $100\ \mu\text{sec}$  [47]. With typical coupling strengths of

$g/2\pi, J/2\pi \sim 200\text{MHz}$ , the evolution time  $T = 15\pi/g \sim 37.5$  nsec. Furthermore, the state initialization pulses in Sec. III can be completed within  $\sim 10$ 's of nsec. These time scales are much shorter than the current decoherence times.

## VI. CONCLUSIONS

To conclude, we studied an optimized nonlinear ramping scheme to prepare the many-body ground states of polaritons in a finite-sized JC lattice. The polaritons are initialized into the ground states in the deep MI and SF regimes via engineered pulse sequence and are subsequently prepared into the many-body ground states in the intermediate regimes of the parameter space by adiabatic ramping. Using a Landau-Zener-type of estimation, we derived the optimal ramping index for given ramping trajectories that can ensure minimal sweeping rate of the Hamiltonian at the energy gap. Our numerical simulation confirmed that the fidelity of the final states can be significantly improved by using the optimal ramping index. We further showed that by choosing an appropriate trajectory, the fidelity can remain close to unity in almost the entire parameter space. We want to emphasize that this approach is general and can be applied to other finite-sized systems. This work can shed lights on high-fidelity preparation of many-body states in engineered quantum systems, such as quantum simulators, and advance the implementation of quantum simulation with NISQ devices.

## VII. ACKNOWLEDGEMENTS

This work is supported by the UC Multicampus-National Lab Collaborative Research and Training under Award No. LFR-17-477237. G.L.L. is supported by the National Natural Science Foundation of China under Grant No. 11974205 and No. 11774197. C.W.W. is also supported by NSF QII-TAQS-1936375, NSF 1919355, and ONR N00014-15-1-2368. L.T. is also supported by UC Merced Faculty Research Grants 2017 and NSF awards No.1720501 and No. 2006076.

---

[1] E. Jaynes and F. Cummings, *Comparison of Quantum and Semiclassical Radiation Theories with Application to the Beam Maser*, Proc. IEEE **51**, 89 (1963).

[2] J. M. Raimond, M. Brune, and S. Haroche, *Manipulating Quantum Entanglement with Atoms and Photons in a Cavity*, Rev. Mod. Phys. **73**, 565 (2001).

[3] S. M. Girvin, in Lecture Notes on *Strong Light-Matter Coupling: from Atoms to Solid-State Systems* (World Scientific, Singapore, 2013).

[4] J. Q. You and F. Nori, *Atomic Physics and Quantum Optics using Superconducting circuits*, Nature **474**, 589 (2011).

[5] M. J. Hartmann, F. G. S. L. Brandão, and M. B. Plenio, *Strongly Interacting Polaritons in Coupled Arrays of Cavities*, Nature Phys. **2**, 849 (2006).

[6] A. D. Greentree, C. Tahan, J. H Cole, and L. C L Hollenberg, *Quantum Phase Transitions of Light*, Nature Phys. **2**, 856 (2006).

[7] D. G. Angelakis, M. F. Santos, and S. Bose, *Photon-Blockade-Induced Mott Transitions and XY Spin Models in Coupled Cavity Arrays*, Phys. Rev. A **76**, 031805(R) (2007).

[8] D. Rossini and R. Fazio, *Mott-Insulating and Glassy Phases of Polaritons in 1D Arrays of Coupled Cavities*, Phys. Rev. Lett. **99**, 186401 (2007).

[9] N. Na, S. Utsunomiya, L. Tian, and Y. Yamamoto, *Strongly Correlated Polaritons in a Two-Dimensional Array of Photonic Crystal Microcavities* Phys. Rev. A **77**, 031803(R) (2008).

[10] J. Koch and K. Le Hur, *Superfluid-Mott-Insulator Transition of Light in the Jaynes-Cummings Lattice*, Phys. Rev. A **80**, 023811 (2009).

[11] A. A. Houck, H. E. Türeci and J. Koch, *On-Chip Quantum Simulation with Superconducting Circuits*, *Nature Physics* **8**, 262 (2012).

[12] Y. Hu and L. Tian, *Deterministic Generation of Entangled Photons in Superconducting Resonator Arrays*, *Phys. Rev. Lett.* **106**, 257002 (2011).

[13] K. Seo and L. Tian, *Quantum Phase Transition in a Multiconnected Superconducting Jaynes-Cummings Lattice*, *Phys. Rev. B* **91**, 195439 (2015).

[14] K. Seo and L. Tian, *Mott Insulator-Superfluid Phase Transition in a Detuned Multi-Connected Jaynes-Cummings Lattice*, *Sci. China Phys. Mech. Astron.* **58**, 1 (2015).

[15] J. Xue, K. Seo, L. Tian, T. Xiang, *Quantum Phase Transition in a Multiconnected Jaynes-Cummings Lattice*, *Phys. Rev. B* **96**, 174502 (2017).

[16] A. J. Hoffman, S. J. Srinivasan, S. Schmidt, L. Spietz, J. Aumentado, H. E. Türeci, and A. A. Houck, *Dispersive Photon Blockade in a Superconducting Circuit*, *Phys. Rev. Lett.* **107**, 053602 (2011).

[17] F. Nissen, S. Schmidt, M. Biondi, G. Blatter, H. E. Türeci, J. Keeling, *Nonequilibrium Dynamics of Coupled Qubit-Cavity Arrays*, *Phys. Rev. Lett.* **108**, 233603 (2012).

[18] M. Fitzpatrick, N. M. Sundaresan, A. C. Y. Li, J. Koch, and A. A. Houck, *Observation of a Dissipative Phase Transition in a One-Dimensional Circuit QED Lattice*, *Phys. Rev. X* **7**, 011016 (2017).

[19] R. P. Feynman, *Simulating Physics with Computers*, *Int. J. Theor. Phys.* **21**, 467 (1982).

[20] S. Lloyd, *Universal Quantum Simulators*, *Science* **273**, 1073 (1996).

[21] A. Aspuru-Guzik, A. D. Dutoi, P. J. Love, and M. Head-Gordon, *Simulated Quantum Computation of Molecular Energies*, *Science* **309**, 1704 (2005).

[22] E. Farhi, J. Goldstone, S. Gutmann, and M. Sipser, *Quantum Computation by Adiabatic Evolution*, arXiv:quant-ph/0001106.

[23] T. Albash and D. A. Lidar, *Adiabatic Quantum Computation*, *Rev. Mod. Phys.* **90**, 015002 (2018), arXiv:1611.04471 [quant-ph].

[24] E. Farhi, J. Goldstone, S. Gutmann, J. Lapan, A. Lundgren, and D. Preda, *A Quantum Adiabatic Evolution Algorithm Applied to Random Instances of an NP-Complete Problem*, *Science* **292**, 472 (2001).

[25] J. Roland and N. J. Cerf, *Quantum Search by Local Adiabatic Evolution*, *Phys. Rev. A* **65**, 042308 (2002).

[26] H. T. Quan and W. H. Zurek, *Testing Quantum Adiabaticity with Quench Echo*, *New J. Phys.* **12**, 093025 (2010).

[27] X. Chen, I. Lizuain, A. Ruschhaupt, D. Guéry-Odelin, and J. G. Muga, *Shortcut to Adiabatic Passage in Two- and Three-Level Atoms*, *Phys. Rev. Lett.* **105**, 123003 (2010).

[28] A. del Campo, M. M. Rams, and W. H. Zurek, *Assisted Finite-Rate Adiabatic Passage Across a Quantum Critical Point: Exact Solution for the Quantum Ising Model*, *Phys. Rev. Lett.* **109**, 115703 (2012).

[29] A. Yu. Kitaev, *Quantum Measurements and the Abelian Stabilizer Problem*, (1995), arXiv:quant-ph/9511026.

[30] D. S. Abrams and S. Lloyd, *Simulation of Many-Body Fermi Systems on a Universal Quantum Computer*, *Phys. Rev. Lett.* **79**, 2586 (1997).

[31] A. Peruzzo, J. McClean, P. Shadbolt, M.-H. Yung, X.-Q. Zhou, P. J. Love, A. Aspuru-Guzik, and J. L. O'Brien, *A Variational Eigenvalue Solver on a Photonic Quantum Processor*, *Nature Commun.* **5**, 4213 (2014).

[32] E. F. Dumitrescu, A. J. McCaskey, G. Hagen, G. R. Jansen, T. D. Morris, T. Papenbrock, R. C. Pooser, D. J. Dean, and P. Lougovski, *Cloud Quantum Computing of an Atomic Nucleus*, *Phys. Rev. Lett.* **120**, 210501 (2018).

[33] S. J. Wei, H. Li, and G. L. Long, “A Full Quantum Eigensolver for Quantum Chemistry Simulations”, *Research* **2020**, 1486935 (2020).

[34] B. Kraus, H. P. Büchler, S. Diehl, A. Kantian, A. Micheli, and P. Zoller, *Preparation of Entangled States by Quantum Markov Processes*, *Phys. Rev. A* **78**, 042307 (2008).

[35] F. Verstraete, M. M. Wolf, and J. I. Cirac, *Quantum Computation and Quantum-State Engineering Driven by Dissipation*, *Nature Physics* **5**, 633 (2009).

[36] J. Preskill, *Quantum Computing in the NISQ Era and Beyond*, *Quantum* **2**, 79 (2018), arXiv:1801.00862 [quant-ph].

[37] C. K. Law and J. H. Eberly, *Arbitrary Control of a Quantum Electromagnetic Field*, *Phys. Rev. Lett.* **76**, 1055 (1996).

[38] D. Sen, K. Sengupta, and S. Mondal, *Defect Production in Nonlinear Quench across a Quantum Critical Point*, *Phys. Rev. Lett.* **101**, 016806 (2008).

[39] S. Mondal, K. Sengupta, and D. Sen, *Theory of Defect Production in Nonlinear Quench across a Quantum Critical Point*, *Phys. Rev. B* **79**, 045128 (2009).

[40] R. Barankov and A. Polkovnikov, *Optimal Nonlinear Passage Through a Quantum Critical Point*, *Phys. Rev. Lett.* **101**, 076801 (2008).

[41] L. D. Landau, *Zur theorie der energieübertragung ii*, *Phys. Z. Sowjetunion* **2**, 46 (1932).

[42] C. Zener, *Non-Adiabatic Crossing of Energy Levels*, *Proc. R. Soc. London. A* **137**, 696 (1932).

[43] C. Neill, P. Roushan, K. Kechedzhi, S. Boixo, S. V. Isakov, V. Smelyanskiy, R. Barends, B. Burkett, Y. Chen, Z. Chen, B. Chiaro, A. Dunsworth, A. Fowler, B. Foxen, R. Graff, E. Jeffrey, J. Kelly, E. Lucero, A. Megrant, J. Mutus, M. Neeley, C. Quintana, D. Sank, A. Vainsencher, J. Wenner, T. C. White, H. Neven, and J. M. Martinis, *A Blueprint for Demonstrating Quantum Supremacy with Superconducting Qubits*, *Science* **360**, 195 (2018).

[44] P. Zhao, Z. Jin, P. Xu, X. Tan, H. Yu, and Y. Yu, *Two-Photon Driven Kerr Resonator for Quantum Annealing with Three-Dimensional Circuit QED*, *Phys. Rev. Applied* **10**, 024019 (2018).

[45] M. H. Devoret and R. J. Schoelkopf, *Superconducting Circuits for Quantum Information: An Outlook*, *Science* **339**, 1169 (2013).

[46] G. Wendin, *Quantum Information Processing with Superconducting Circuits: A Review*, *Rep. Prog. Phys.* **80** 106001 (2017);

[47] P. Krantz, M. Kjaergaard, F. Yan, T. P. Orlando, S. Gustavsson, and W. D. Oliver, *A Quantum Engineer's Guide to Superconducting Qubits*, *Appl. Phys. Rev.* **6**, 021318 (2019).

[48] F. Mei, V. M. Stojanovic, I. Siddiqi, L. Tian, *An analog superconducting quantum simulator for Holstein polarons*, *Phys. Rev. B* **88**, 224502 (2013).

[49] O. Penrose and L. Onsager, *Bose-Einstein Condensation and Liquid Helium*, *Phys. Rev.* **104**, 576 (1956).

[50] C. N. Yang, *Concept of Off-Diagonal Long-Range Order and the Quantum Phases of Liquid He and of Superconductors*, *Rev. Mod. Phys.* **34**, 694 (1962).